

# Inference of biological and physical parameters in an internal wave using multiple-frequency, acoustic-scattering data

Joseph D. Warren, Timothy K. Stanton, Peter H. Wiebe, and Harvey E. Seim

Warren, J. D., Stanton, T. K., Wiebe, P. H., and Seim, H. E. 2003. Inference of biological and physical parameters in an internal wave using multiple-frequency, acoustic-scattering data. – ICES Journal of Marine Science, 60: 1033–1046.

High-frequency sound (>10 kHz) is scattered in the ocean by many different processes. In the water column, marine organisms are often assumed to be the primary source of acoustic backscatter. Recent field experiments and theoretical work suggest that the temperature and salinity microstructure in some oceanic regions could cause acoustic scattering at levels comparable to that caused by marine life. Theoretical acoustic-scattering models predict that the scattering spectra for microstructure and organisms are distinguishable from each other over certain frequency ranges. A method that uses multiple-frequency acoustic data to exploit these differences has been developed, making it possible to discriminate between biological and physical sources of scattering under some conditions. This method has been applied to data collected in an internal wave in the Gulf of Maine. For regions of the internal wave in which the dominant source of scattering is either biological or physical in origin, it is possible to combine the acoustic-scattering data and temperature and salinity profiles with acoustic-scattering models to perform a least-squares inversion. Using this approach, it is possible to estimate the dissipation rate of turbulent kinetic energy for some regions of the internal wave, and the length and numerical abundance of the dominant biological scatterer, euphausiids, in others.

© 2003 International Council for the Exploration of the Sea. Published by Elsevier Ltd. All rights reserved.

Keywords: acoustics, inverse methods, microstructure, zooplankton.

Received 31 July 2002; accepted 31 December 2002.

*J. D. Warren, T. K. Stanton, and P. H. Wiebe: Woods Hole Oceanographic Institution, Woods Hole, MA 02543, USA. H. E. Seim: University of North Carolina, Chapel Hill, NC 27599, USA. Correspondence to J. D. Warren, Southampton College, Southampton, NY 11968, USA; tel: +1 631 287 8390; fax: +1 631 287 8419; e-mail: [joe.warren@liu.edu](mailto:joe.warren@liu.edu).*

## Introduction

Acoustic-scattering methods offer biologists a useful tool in estimating the distribution and abundance of marine organisms that scatter a measurable amount of sound, such as fish and zooplankton (e.g. Dietz, 1948; Castile, 1975; Holliday and Pieper, 1995). Acoustic surveys of the water column can provide information at sub-meter resolution over a range of several hundred meters from the echosounder, as well as covering horizontal distances of the order of 10s–100s of kilometers. Thus, acoustic techniques allow a significantly larger area of the ocean interior to be surveyed at a finer resolution than traditional methods of surveying biomass such as net tows, video (which has high resolution but low sampling volume), or diver observations. However, acoustical surveys measure the amount of

scattered sound in the water column and are not a direct measure of the biological organisms present. Several studies have begun to address the complex problem of how to convert the measured backscattered energy into estimates of zooplankton biomass (Holliday and Pieper, 1995; Wiebe *et al.*, 1997; Brierley *et al.*, 1998).

There are other objects or processes in the ocean that can scatter detectable amounts of sound. Suspended sediments, air bubbles, and even gradients of temperature, salinity, and the velocity of the water column itself can scatter acoustic energy and cause difficulty in interpreting the acoustic data. Temperature and salinity microstructure occurs throughout the oceans and the mixing processes that cause and result from the microstructure are of interest to physical oceanographers (Gregg, 1987; Thorpe, 1987). In many cases, turbulence in the water column produces these temperature

and salinity variations and also detectable amounts of acoustic backscatter (Woods, 1977). High-frequency acoustic measurements were suggested as a means of studying turbulence several decades ago (Batchelor, 1959). However, to test this hypothesis theoretical models describing the acoustic scattering from these physical processes as well as experimental measurements are required. These scattering models have inputs which parameterize the turbulence, such as  $\epsilon$  and  $\chi$  (the dissipation rates of turbulent kinetic energy and temperature variance, respectively); however, other non-turbulent processes (such as salt fingers) can also produce microstructure (Gregg, 1987; Schmitt, 1994).

Internal waves are a common feature throughout the oceans and are associated with high values of turbulence (Sandstrom *et al.*, 1989; Hebert *et al.*, 1992). These waves propagate along density gradients and commonly have amplitudes of tens of meters. It is thought that internal waves may play a role in the aggregation or transportation of zooplankton (Lennert-Cody and Franks, 1999). Internal waves have frequently been observed acoustically (Hauray *et al.*, 1983; Sandstrom *et al.*, 1989; Wiebe *et al.*, 1997; Trevorrow, 1998; Orr *et al.*, 2000), and some of these studies have inferred the source (biological or physical) of the scattering. One of the major limitations of the previous studies is the fact that generally only a single-frequency echosounder was used or the spectral characteristics of the scattering were not exploited when more than one frequency was involved.

Theoretical models of acoustic-scattering spectra from biological- and physical-scattering processes have different shapes (Figure 1) (Stanton *et al.*, 1994b). These differences make it possible for a multiple-frequency acoustic system used in a field survey to differentiate and measure the scattering contributions from these processes. In this study, a multiple-frequency acoustic system was used to survey a region where both biological and physical sources of scattering were present. The differences of the scattering spectra from different regions of the water column were used to infer the dominant source of scattering. Scattering models and measurements of the biota and hydrography were used to estimate the size and numerical density of the dominant biological sound scatterer as well as the dissipation rate of turbulent kinetic energy.

## Methods

The acoustic survey was conducted in the eastern part of Wilkinson Basin (located north of Georges Bank and east of Stellwagen Bank) in the Gulf of Maine on 16 October 1997 (Figure 2). Internal waves have been observed in this area previously and are thought to be formed by the accumulation of water on the shallow banks (Georges and Stellwagen) during the tidal cycle. Tidally-driven interaction of density-stratified water with the shallows forms a lee wave that is released from the bank and propagates along the pycnocline into deeper water (Hauray *et al.*, 1979).

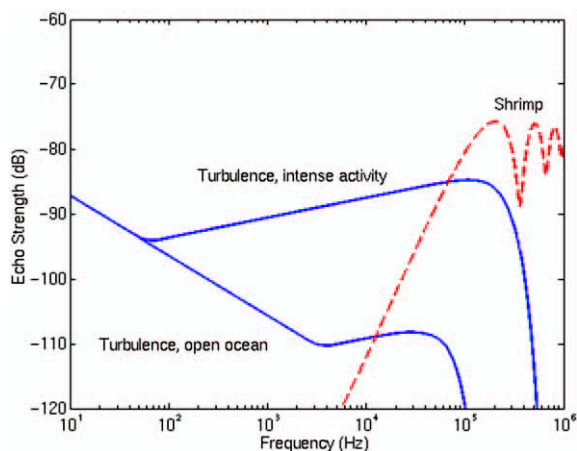


Figure 1. Theoretical predictions of echo strength versus frequency for turbulence and a 2-cm long shrimp. The curves for turbulence are from Goodman (1990), while the shrimp curve is from Stanton *et al.* (1993). Curves are presented so that the scattering from  $1 \text{ m}^3$  of turbulence (“volume-scattering strength”) can be directly compared to the scattering from a shrimp (“target strength”) with a numerical density of  $1 \text{ animal m}^{-3}$ . Figure re-drawn from Stanton *et al.* (1994b).

To provide spectral information about the scattering processes occurring in the water column, acoustic-backscatter data were collected by BIO-Optical Multi-frequency Acoustical and Physical Environmental Recorder (BIO-MAPER-II). Three transects were made through the internal-wave field during the experiment. Before the first transect, conductivity, temperature, and depth (CTD) cast # 10 was conducted. Immediately after the third transect was completed, Multiple Opening and Closing Net and Environmental Sensing System (MOCNESS) tow # 9 was performed. These three data sets provide the information needed to analyze the separate contributions from the biological and physical sources of acoustic scattering.

## Acoustic data

BIOMAPER-II is a towed body with numerous acoustic, environmental, video, and optical sensors (Wiebe *et al.*, 2002). The calibrated acoustic system comprises five pairs of transducers (operating at 43, 120, 200, 420, and 1000 kHz), with one of each frequency looking upward and the other downward. The instrument is typically “tow-yoed” through the water column to depths within 20 m of the sea floor. The data discussed herein were collected with BIOMAPER-II towed at a constant depth just beneath the surface. Data are only from the downward-looking transducers. Typical horizontal tow speeds were between 4 and 6 knots. The system was programmed to record acoustic data to ranges of 200, 200, 150, 100, and 35 m (relative to the aforementioned frequencies) from the echosounder with a depth-bin size of 1 m. Backscattered energy from each transducer and for each depth bin was recorded as

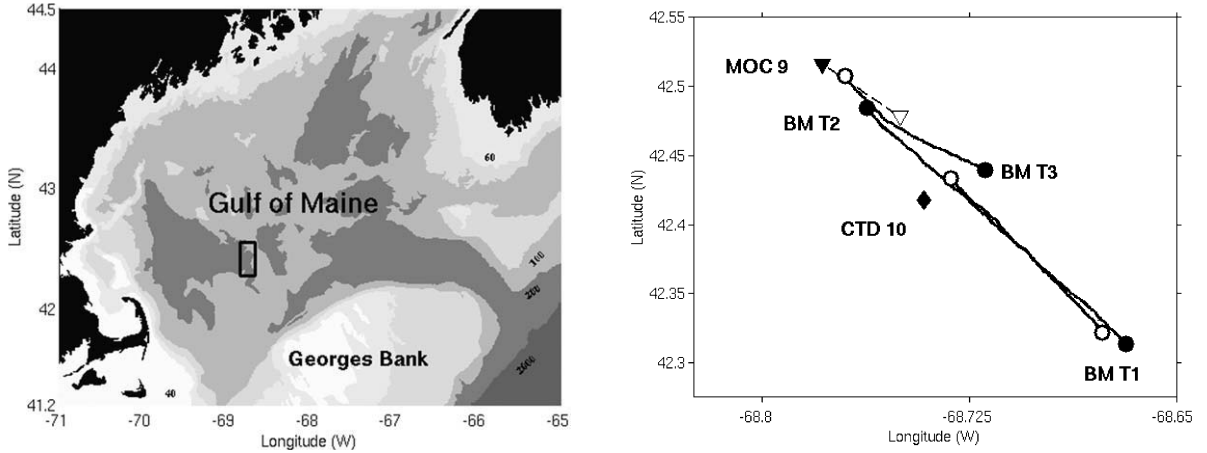


Figure 2. Bathymetry of the Gulf of Maine showing the location of the internal wave study (left). Location of the CTD profile (diamond), MOCNESS tow (triangles), and acoustic transects (BM T1–3) of the internal wave (right). Open and closed symbols represent the start and end points, respectively, of the transects. Labels appear next to the end point of each transect. Table 1 provides the beginning- and end-time information for each sampling event.

echo-integrated volume-backscattering strength ( $S_v$ , in dB re  $1 \text{ m}^{-1}$ ) every 12 s. The acoustic-data files were combined with data from the Environmental Sensing System (ESS) sensors, which were located onboard BIOMAPER-II. The final data file provided volume-scattering strength for the water column along with position (latitude, longitude, and instrument depth), temperature, salinity, fluorescence, turbidity, and other sensor data.

## Models and sampling

### Zooplankton-scattering model

In order to estimate the acoustic energy scattered from aggregations of zooplankton, it is vital to know how much energy an individual animal scatters. Much research has been conducted on developing mathematical models that combine scattering physics and geometrical models of animal shape for various types of zooplankton (see reviews: Holliday and Pieper, 1995; Foote and Stanton, 2000). These models have been compared with measurements of scattering from individual animals in laboratory studies (McGehee *et al.*, 1998; Stanton *et al.*, 1998).

The dominant biological sound scatterers in the Gulf of Maine are often the fluid-like, elongated zooplankton such as decapod shrimp and euphausiids. The target strength (TS) of these animals can be modeled with the equation from Stanton *et al.* (1994a) for randomly oriented, bent, fluid cylinders

$$TS = 10 \log \left( 0.32R^2 a^2 \beta_D \times \left[ 1 - e^{-8(ka)^2 s_d^2} \cos \left( ka \left( 4 - \frac{\pi}{ka + 0.8} \right) \right) \right] \right) \quad (1)$$

where  $a$  is the radius of the animal (in m) and  $k$  is the acoustic wavenumber ( $k = 2\pi f/c$ ) which is a function of the acoustic frequency ( $f$  in Hz) and the speed of sound in seawater ( $c = 1500 \text{ m s}^{-1}$ ). The other parameters are fixed values determined by previous studies and empirical methods: reflection coefficient ( $R = 0.058$ ), length-to-diameter ratio ( $\beta_D = 5.36$ ), and the standard deviation of length divided by the average length ( $s_d = 0.06$ ) (Stanton *et al.*, 1993, 1994a). This equation describes the back-scattered energy averaged over all angles of orientation and a narrow distribution of length. It has been successfully applied to data from both laboratory experiments (Stanton *et al.*, 1993, 1994a) and field surveys (Wiebe *et al.*, 1996, 1997).

### Zooplankton sampling

Zooplankton were sampled with a  $1 \text{ m}^2$  MOCNESS (Wiebe *et al.*, 1985) tow conducted immediately after the acoustic transect of the internal wave (Table 1). A MOCNESS system comprises a series of nine nets; when the first net is closed, the second net is opened, and so on. This procedure allowed for specific depth strata to be surveyed. Generally, net #0 was open from the surface to the deepest point of the tow (10–20 m above the bottom), the remaining nets (#1–8) were opened and closed in succession every 25–50 m during the return to the surface. The MOCNESS system also recorded the volume of water filtered by each net, the time that each net was opened and closed, depth, salinity, temperature, density, and fluorescence.

The nets were equipped with  $335\text{-}\mu\text{m}$  mesh and cod-end buckets for collection of zooplankton and larval fish. Each cod-end sample was then split and preserved in a buffered formalin solution. Samples were processed after the cruise

Table 1. Event log for the internal-wave survey from “Endeavor” on 16 October 1997. Three transects of the internal wave were made with BIOMAPER-II at different depths. Only data from the first transect (BM Pass 1) are discussed in this work.

Event	Julian Day	Latitude (N)	Longitude (W)	Begin/end
CTD 10	289.535	42°25.08′	68°44.49′	Begin
CTD 10	289.562	42°25.08′	68°44.49′	End
BM Pass 1	289.58	42°25.638′	68°44.04′	Begin
BM Pass 1	289.67	42°18.528′	68°40.164′	End
BM Pass 2	289.68	42°19.326′	68°40.608′	Begin
BM Pass 2	289.77	42°29.07′	68°45.714′	End
BM Pass 3	289.80	42°31.794′	68°46.554′	Begin
BM Pass 3	289.87	42°26.376′	68°43.152′	End
MOC 09	289.896	42°28.70′	68°45.00′	Begin
MOC 09	289.949	42°30.97′	68°46.69′	End

by silhouette photography. These photographs were then examined under a microscope and the biological organisms were measured and identified by taxonomic group (Davis and Wiebe, 1985). Animal density (number of animals  $m^{-3}$ ) was calculated for each net for each taxonomic group.

#### Microstructure-scattering model

Variations in temperature and salinity cause changes in the acoustical impedance of the medium, which is a function of both the density ( $\rho$ ) and the index of refraction ( $\eta$ ). This in turn leads to scattering. Under a number of circumstances scattering due to the index of refraction fluctuations dominates, and the contribution from fluctuations in the density can be ignored. This is the case for the data in question here since the temperature microstructure is stronger than the salinity microstructure. Under these circumstances it can be shown that the scattering cross-section per unit volume ( $\sigma$ ) for energetic, homogeneous, and isotropic turbulence is proportional to the three-dimensional wavenumber spectrum of index of refraction fluctuations (Goodman, 1990):

$$\sigma = 2\pi k^4 \Phi_\eta(k_{br})$$

where  $k_{br}$  is the Bragg wavenumber ( $k_{br} = 2k$  for backscattering), and  $\Phi_\eta(k_{br})$  is the three-dimensional, wavenumber spectrum of index of refraction fluctuations evaluated at the Bragg wavenumber. The wavenumber spectrum of index of refractions fluctuations can then be related to the one-dimensional wavenumber spectra of temperature ( $\Phi_T$ ) and salinity ( $\Phi_S$ ); and the co-spectrum of temperature and salinity ( $\Phi_{ST}$ ), evaluated at the Bragg wavenumber (Seim *et al.*, 1995). Thus for backscattering, where  $k_{br} = 2k$ ,

$$\sigma_{bs} = -\frac{k_{br}^3}{32} \frac{d}{dk} [a^2 \Phi_T + b^2 \Phi_S + 2ab \Phi_{ST}] \quad (2)$$

where  $a$  and  $b$  are the relative importance of temperature and salinity to variations in sound speed, respectively

$$\left( a = \frac{1}{c} \frac{\partial c}{\partial T} \Big|_{S,T} \quad b = \frac{1}{c} \frac{\partial c}{\partial S} \Big|_{S,T} \right). \quad (3)$$

Bragg scattering occurs when scattering contributions from different facets are in-phase with each other. In this case, the facets are the interfaces of the microstructure layers. When the direction of propagation of the incident acoustic wave is perpendicular to these surfaces then the separation of these layers for Bragg scattering to occur is equal to half a wavelength. If the variations in temperature and salinity occur on scales near this  $\lambda/2$  separation distance, then constructive interference will occur resulting in a peak in the scattering spectrum.

To evaluate the backscattering cross-section per unit volume given by Equation (2) it is necessary to know the wavenumber spectra of temperature and salinity, as well as their co-spectrum. A model proposed by Seim (1999) based on a Batchelor spectrum for temperature and salinity is used. The one-dimensional wave spectra, and thus the scattering model, are divided into two regions: an inertial-convective model for wavenumbers below  $k = k_*$  ( $k_*$  is where the inertial-convective and viscous-convective sub-ranges intersect) and a viscous-convective model for wavenumbers above  $k_*$ . Since there is little information about the form of the temperature and salinity co-spectrum, we follow Seim (1999) and use an upper bound for the co-spectrum. This upper bound represents a perfect correlation between temperature and salinity fluctuations. In some situations (as discussed in Seim, 1999), this upper-bound assumption will not be true and the co-spectrum term will vary and cause changes in the shape of the scattering spectra. However, given the uncertainty in the actual form of the co-spectrum, the upper bound assumption was used. Thus the Seim (1999) microstructure-scattering model is:

$$\sigma_{bs} = A \frac{5}{96} \frac{\chi}{\varepsilon^{1/3}} k_{br}^{1/3} \left( a^2 + \frac{b^2}{\delta^2} + \frac{2ab}{\delta} \right) \text{ for } k \leq k_{int} \quad (4)$$

$$\sigma_{bs} = \frac{q}{32} \left( \frac{\nu}{\varepsilon} \right)^{1/2} \chi k_{br} \times \left[ a^2 e^{-\zeta^2/2} + \frac{b^2}{\delta^2} e^{-\zeta_s^2/2} + \frac{ab\Gamma}{\delta [g(\zeta)g(\zeta_s)]^{1/2}} \right] \text{ for } k > k_{int} \quad (5)$$

where

$$\Gamma = \left( \frac{D_s}{D} \right)^{1/4} g(\zeta) e^{-\zeta^2/2} + \left( \frac{D}{D_s} \right)^{1/4} g(\zeta_s) e^{-\zeta_s^2/2}. \quad (6)$$

The parameter  $A$  is equal to 0.925 such that the wavenumber spectra in the two regions are equal at  $k_*$  (Seim, 1999) and  $q$  is 3.7 as suggested by Oakey (1982). Additional model inputs are given in Table 2. In order to evaluate  $\sigma_{bs}$  as a function of frequency and depth it is

Table 2. Parameters of the microstructure-scattering model given in Equations (4)–(6).

Parameter	Description	Units
$\varepsilon$	Dissipation rate of turbulent kinetic energy	$\text{W kg}^{-1}$
$\chi$	Dissipation rate of temperature variance	$^{\circ}\text{C}^2 \text{s}^{-1}$
$\delta = \left( \frac{\partial T}{\partial z} / \frac{\partial s}{\partial z} \right)$	Ratio of the vertical gradients of T and S	$^{\circ}\text{C psu}^{-1}$
$k_* = \frac{\left( \frac{\varepsilon}{\nu^3} \right)^{1/4}}{8}$	Transverse shear spectrum peak wavenumber	$\text{m}^{-1}$
$k_{\text{int}} = \left( \frac{5}{3} \right)^{3/2} k_*$	Wavenumber dividing inertial-convective and viscous-convective models	$\text{m}^{-1}$
$k_d = \left( \frac{\varepsilon}{\nu D^2} \right)^{1/4}, \quad k_{ds} = \left( \frac{\varepsilon}{\nu D_s^2} \right)^{1/4}$	Diffusive cutoff wavenumber for T, S	$\text{m}^{-1}$
$\zeta = (2q)^{1/2} \frac{k}{k_d}, \quad \zeta_s = (2q)^{1/2} \frac{k}{k_{ds}}$	Non-dimensional spatial wavenumber	1
$g(\zeta) = \zeta \left[ e^{-\frac{\zeta^2}{2}} - \zeta \int_{\zeta}^{\infty} e^{-\frac{x^2}{2}} dx \right]$	“Universal” spectrum	1
$\nu \sim 1 \times 10^{-6}$	Mean dynamic viscosity	$\text{m}^2 \text{s}^{-1}$
$D \sim 1 \times 10^{-7}$	Mean scalar diffusivity for temperature	$\text{m}^2 \text{s}^{-1}$
$D_s \sim 1 \times 10^{-9}$	Mean molecular diffusivity of salinity	$\text{m}^2 \text{s}^{-1}$
T(z)	Temperature	$^{\circ}\text{C}$
S(z)	Salinity	psu

necessary to obtain profiles of temperature, salinity, and the dissipation rates of turbulent kinetic energy and temperature variance. For this analysis, the temperature and salinity profiles were obtained from CTD #10. However, it is clear from Equations (4)–(6) that it is critical to obtain profiles of  $\chi$  and  $\varepsilon$  to accurately predict acoustic scattering from microstructure using this model. It is difficult to adequately sample microstructure from a towed instrument, such as BIOMAPER-II. Ideally, sensors that can rapidly respond to cm-scale fluctuations through which they are being towed are mounted on a vibration-free instrument (Oakey, 1988). Furthermore, a suite of sensors should be used spanning measurements of temperature, salinity, and three-dimensional fluid velocities which would allow for direct calculations of microstructure and turbulence parameters (such as  $\varepsilon$  and  $\chi$ ). However, the BIOMAPER-II and

MOCNESS systems currently do not have these capabilities. Instead, indirect methods of estimating these inputs to the scattering model will be made from CTD-cast data sampled at 24 Hz with a vertical resolution of a few cm (as opposed to the 0.25 Hz sampling rate of the BIOMAPER-II-based CTD system which produced a vertical resolution of approximately 50 cm).

#### Microstructure sampling

Profiles of temperature and salinity were used to estimate the parameters associated with microstructure for the acoustic-scattering model for microstructure. A full description of the method for estimating  $\varepsilon$  is provided by Dillon (1982), which details how to use instabilities in the density profile of the water column to provide a scaling, the Thorpe length ( $L_T$ ). This scale has been found to be

proportional to the Ozmidov length which in turn is proportional to the dissipation rate of turbulent kinetic energy. The Thorpe length can be found by reordering the density profile such that it is stable (higher-density water is deeper than lower-density water). The Thorpe length is simply the root-mean-square vertical displacement that a water parcel would undergo in moving from the measured profile to a stable profile. The Thorpe-length calculations are averaged over multiple depth bins (selected by hand) in the water column, in order to reduce the variability.

Once the Thorpe length has been found, it can be related to the Ozmidov scale,  $L_o$ . Dillon (1982) showed that for three different oceanic conditions the Thorpe length was directly proportional to the Ozmidov length by the relationship

$$L_o(z) = 0.8L_T(z) \quad (7)$$

and the Ozmidov length is a function of the dissipation rate of turbulent kinetic energy and the buoyancy frequency ( $N$ )

$$L_o(z) = \left( \frac{\varepsilon(z)}{N^3(z)} \right)^{1/2} \quad (8)$$

The buoyancy frequency is found by using the gradient of the density profile

$$N^2(z) = -\frac{g}{\rho(z)} \frac{\partial \rho(z)}{\partial z} \quad (9)$$

where  $\rho$  is the fluid density,  $g$  the acceleration due to gravity, and  $z$  is the vertical coordinate and is positive upward. Once the Thorpe length is estimated, then  $\varepsilon$  can be found by combining the above equations. It should be noted that these estimates for  $\varepsilon$  should be considered rough values, and are used only because there were no instruments aboard to make direct measurements of these inputs.

While it is possible to estimate  $\chi$  by assuming that it is a function of  $\varepsilon$  and other parameters, initial results from this approach produced values of  $\chi$  that were unreasonably large. From Equations (4) and (5), it is clear that varying  $\chi$  changes the amplitude of the  $\sigma_{bs}$  prediction, but not the frequency dependence. Therefore, in order to reduce the variability in the model output,  $\chi$  was set to a constant value of  $1 \times 10^{-6} \text{ } ^\circ\text{C}^2 \text{ s}^{-1}$ .

#### Acoustic discrimination between physical and biological processes

A method to quantify the shape of the scattering-strength spectrum is needed to distinguish between biological and physical scatterers, so for a specific latitude, longitude, and depth a first-order polynomial (straight line) was fitted to the volume-backscattering strength at 43, 120, 200, and 420 kHz. The 1 MHz data were limited to a range of 35 m and were not included in this analysis so that a larger portion of the water column could be studied. The slope of this line was then calculated. These slope measurements are not intended to describe the physics of the scattering processes, but rather act as a crude parameter to differentiate

them. There are several difficulties with this approach, including the fact that this method is limited to the range of the highest-frequency echosounder (in this case 100 m). Further complicating the interpretation of these measurements is that the theoretical spectra can have either positive or negative slopes depending on the number and range of acoustic frequencies used, the size distribution of biological scatterers, and the level of microstructure in the water column. To resolve this difficulty, theoretical scattering models were used to determine the limits of applicability of this approach.

For the frequency range used (43–420 kHz), theoretical-scattering spectra for biological scatterers ranging in length from 1 mm to 5 cm produced slope values ranging between  $-1.5 \times 10^{-5}$  and  $3.8 \times 10^{-4} \text{ dB Hz}^{-1}$ . For the microstructure-scattering model, slope values were between  $-2.7 \times 10^{-5}$  and  $1.4 \times 10^{-5} \text{ dB Hz}^{-1}$  for values of  $\varepsilon$  ranging from  $1 \times 10^{-10}$  to  $1 \times 10^{-4} \text{ W kg}^{-1}$ . From this analysis, slope predictions greater than  $1.4 \times 10^{-5}$  were considered to be from regions dominated by biological scatterers, while values less than  $-1.5 \times 10^{-5}$  were from areas dominated by physical-scattering processes. It was difficult to interpret slope measurements that fell between  $-1.5 \times 10^{-5}$  and  $1.4 \times 10^{-5} \text{ dB Hz}^{-1}$  since biological scatterers greater than 2 cm in length, dissipation rates of turbulent kinetic energy greater than  $1 \times 10^{-5}$ , and regions containing both biological- and physical-scattering processes have slopes that fall within this range. Since the dominant scattering process could not be identified, these regions were not analyzed further in this work. However, for areas where one scattering mechanism was found to be dominant, the shape of the measured-scattering spectra was used to provide further information about the scattering process.

#### Inversion of acoustic data for biological and physical parameters

Theoretical zooplankton or microstructure-scattering spectra were fitted to measured spectra using a two-step approach. The key parameter used in fitting the measured spectra is the sharp transition, or “turning point”, from the Rayleigh-scattering regime ( $ka \ll 1$ ) to the geometric-scattering regime ( $ka \gg 1$ ) (roughly between 50 and 300 kHz in Figure 1). For biological-scattering models, the size (or length) of the animal controls the location of the “turning point” which generally occurs near  $ka = 1$ . The scattering model for microstructure also contains a “turning point”, specifically the peak in the spectra associated with Bragg resonance. The location of this peak relative to acoustic frequency is determined by  $\varepsilon$ .

In order to simplify the inversion process, differences in amplitude between the theoretical and measured spectra were ignored and the spectra curves were fitted based on the location of the “turning point”. To determine the best-fit of the scattering curves, parabolas were least-squares fitted to theoretical scattering spectra for either varying animal

lengths or dissipation rates. These parabolas were then correlated with a parabola fitted to the measured scattering data. The “theoretical” parabola with the best-fit was used to characterize the measured scattering data. The parameters of the theoretical scattering model then provide either estimates of the size of the scatterer for biologically dominated scattering regimes, or estimates of  $\epsilon$  for those regions dominated by scattering from physical microstructure.

The second step in the acoustic-inversion process was to use the differences in amplitude between the measured and theoretical scattering curves to obtain more information about the scattering processes. If multiple animals of the same size are located within a given volume, then the theoretical scattering curve for that region will shift upward and predict higher scattering levels, but the location of the “turning point” of the curve will not change. Using the difference in measured and theoretical scattering, estimates of the numerical density of biological scatterers were made. Assuming there are no multiple-scattering effects and no other scatterers are present in the water column, the numerical density of animals (number of animals  $m^{-3}$ ) can be found by

$$n_b = \frac{S_v}{\sigma_{bs}} = \frac{10^{S_v/10}}{10^{TS/10}} = 10^{(S_v - TS)/10} \quad (10)$$

where  $s_v$  is the volume-backscattering coefficient ( $S_v = 10 \log(s_v)$ ) and TS is the predicted target strength for the biological scatterer ( $TS = 10 \log(\sigma_{bs})$ ). Similarly, for scattering from microstructure, changes in the value of  $\chi$  in the model will affect the amplitude but not the “turning point” of the scattering curve. However, given the uncertainty in our method for estimating  $\epsilon$ , no estimates of  $\chi$  were made using this approach.

## Results

Acoustic echograms of the internal wave show two layers with different dependencies of volume-scattering strength upon acoustic frequency (Figure 3). The upper layer was approximately 10–30 m deep and the measured  $S_v$  of the layer decreased with increasing acoustic frequency. The lower layer was approximately 50–70 m deep and the measured  $S_v$  of the layer increased as the acoustic frequency increased. An average value of  $S_v$  for each layer was found by averaging over bins 3 m deep and 150 m in horizontal extent that tracked the centerline of each layer (Figure 4). The scattering spectra for these two layers is consistent with theoretical spectra for temperature and

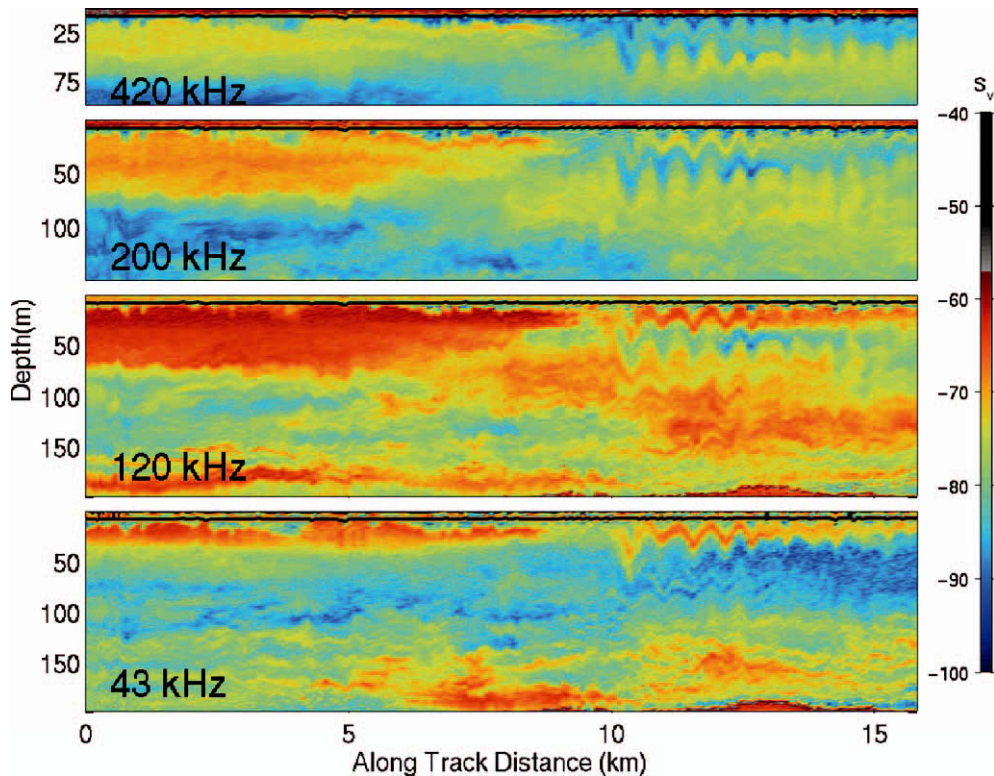


Figure 3. Multiple-frequency acoustic-backscatter data collected by BIOMAPER-II from the internal-wave survey. The internal wave (observed from 10 to 15 km in along-track distance) has two layers which have different scattering strengths at different frequencies.

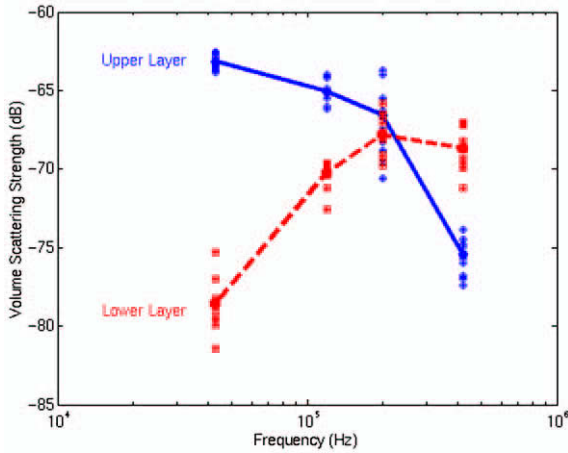


Figure 4. Measured values of  $S_v$  at four frequencies (43, 120, 200, and 420 kHz) from the upper and lower layers of the internal wave. The upper layer has a scattering spectrum which decreases with frequency, while the lower layer has an increasing scattering spectrum. Circles and squares (upper and lower layers, respectively) represent average  $S_v$  values for a 3-m depth bin that tracked the centerline of each layer, while the lines are drawn through the mean value for the upper (full) and lower (dashed) layers.

salinity microstructure (upper layer) and a fluid-like biological scatterer (lower layer) (Figure 1).

The “slope” of the measured-scattering spectra was calculated for this transect for the upper 100 m of the water column (Figure 5). Data-bin size is 1 m vertically and approximately 75 m horizontally. The upper layer of the internal wave had a negative spectral slope, consistent with that of scattering caused by physical processes (Figure 1). In contrast, the lower layer had a positive spectral slope which is consistent with that for scattering from biological processes.

Data from CTD cast #10 show a region of instability probably due to mixing from 5 to 20 m deep (Figure 6). The temperature and salinity data from this CTD profile were used to create theoretical scattering spectra curves for 56 values of  $\epsilon$  (ranging from  $10^{-10}$  to  $10^{-4}$   $\text{W kg}^{-1}$ ) (Figure 7). The measured scattering spectra of the upper layer of the internal wave was best-fit (using a least-squares method) to the theoretical scattering spectra to obtain an estimate of  $\epsilon = 5 \times 10^{-7}$   $\text{W kg}^{-1}$  for the upper layer of the internal wave (Figure 8). Various inversion algorithms are available for analyzing these data, however, since only four frequencies were used a very stable approach is the least-squares method, which is a zeroth-order inversion.

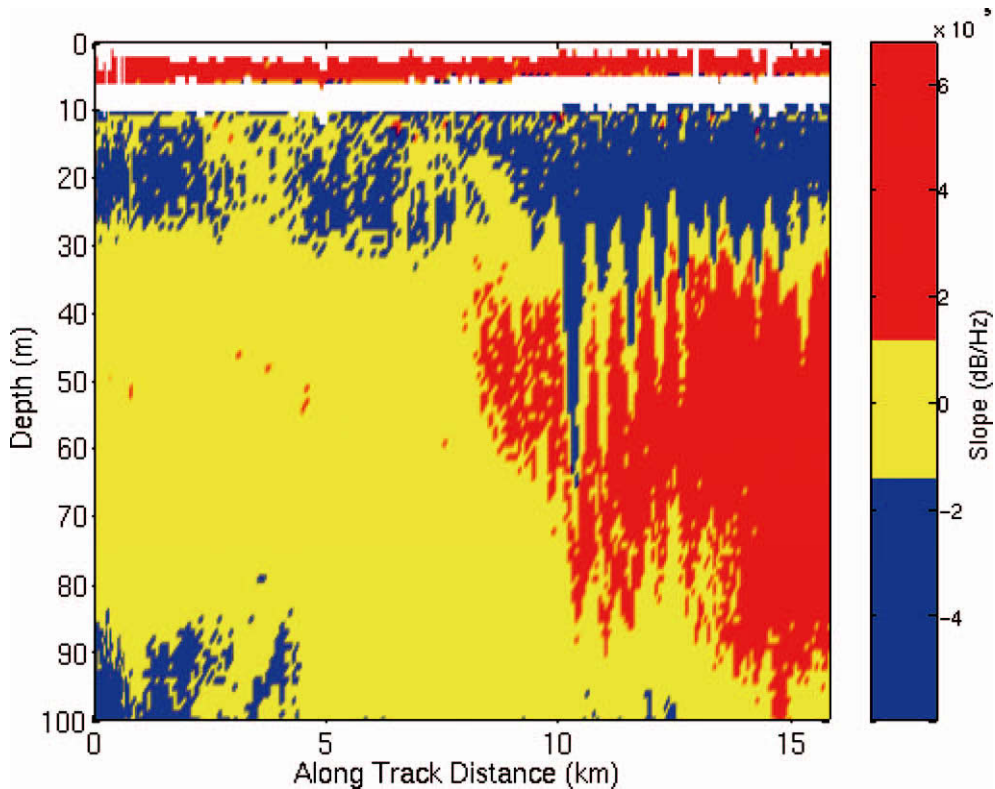


Figure 5. Spectral slope ( $S_v$  versus frequency) calculated from acoustic-backscatter data at 43, 120, 200, and 420 kHz. The internal wave is divided into distinct regions which have slopes consistent with either biological-scattering processes (red, slope  $> 1.4 \times 10^{-5}$   $\text{dB Hz}^{-1}$ ), physical-scattering processes (blue, slope  $< -1.5 \times 10^{-5}$   $\text{dB Hz}^{-1}$ ), or both biological- and physical-scattering processes (yellow,  $-1.5 \times 10^{-5}$   $\text{dB Hz}^{-1} < \text{slope} < 1.4 \times 10^{-5}$   $\text{dB Hz}^{-1}$ ). The data from 0 to 10-m depth may be contaminated by bubbles or surface waves.

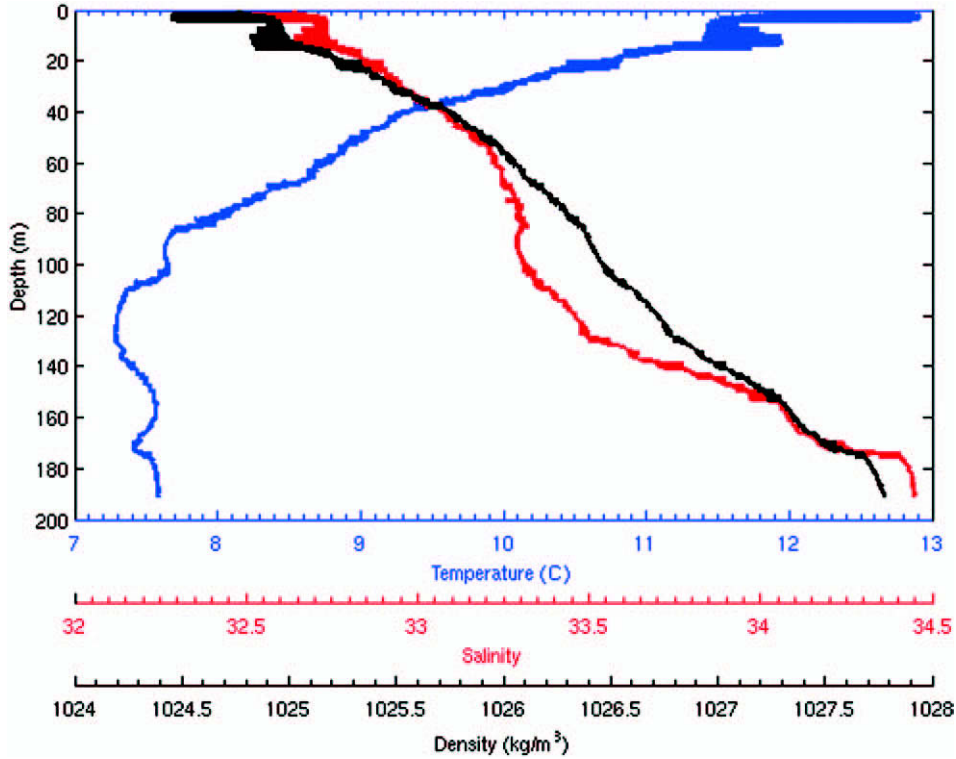


Figure 6. Temperature (blue), salinity (red), and density (black) profiles from CTD #10 taken immediately before the internal-wave survey. Large-scale variations occur in the upper 20 m of the water column which are probably due to mixing by the internal wave.

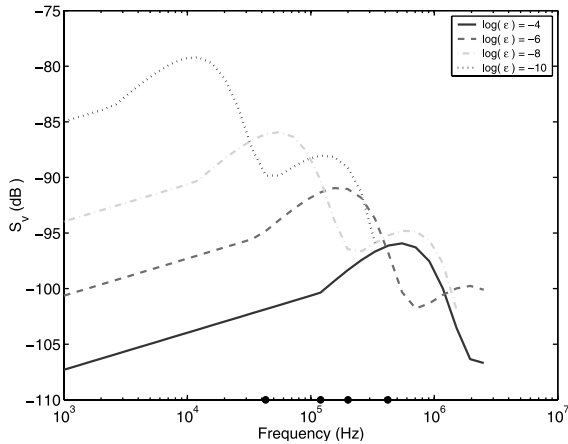


Figure 7. Theoretical scattering spectra for a wide range of dissipation rates of turbulent kinetic energy ( $\epsilon = 10^{-10} - 10^{-4} \text{ W kg}^{-1}$ ) calculated using Equations (4)–(6). Changes in the value of the dissipation rate of temperature variance ( $\chi$ ) affects only the magnitude of these curves (moving the curves vertically), while changes in  $\epsilon$  alter the frequency dependence (moving the curves horizontally). In order to make the inversion analysis more tractable, a fixed value for the dissipation rate of scalar variance ( $\chi = 1 \times 10^{-6} \text{ }^\circ\text{C}^2 \text{ s}^{-1}$ ) was used for all model runs. Solid dots on the horizontal axis mark the acoustic frequencies used by BIOMAPER-II.

This estimate of  $\epsilon$  is consistent with those obtained with microstructure probes (Seim, 1999) in a similar region (the southern edge of Georges Bank and the continental shelf) (Table 3). Few studies have measured the value of  $\epsilon$  in an

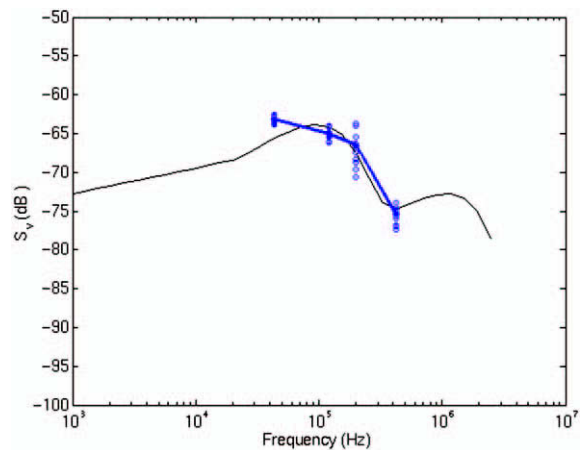


Figure 8. Measured scattering spectra from the upper layer of the internal wave (thick line) least-squares fit to the theoretical scattering spectra for temperature and salinity microstructure. Theoretical curves were offset in amplitude such that the fit was based only on the “turning point” of the curve which is a function of  $\epsilon$ . The theoretical curve with the best-fit was for  $\epsilon = 5 \times 10^{-7} \text{ W kg}^{-1}$ .

Table 3. Estimates of biological- and physical-scattering process parameters from inversion of multiple-frequency, acoustic-backscatter data,  $\epsilon$  was estimated using data from the upper layer of the internal wave, while the measured values are from a study of the New England Shelf with similar temperature and salinity changes ( $2^{\circ}\text{C}$  and  $0.2$ ) separating the upper mixed layer (Figure 1a in Seim, 1999). Animal length and numerical density of euphausiids (assumed to be the dominant biological scatterer) were estimated from data from the lower layer of the internal wave. Measured values of euphausiid length and numerical density are from animal samples collected in the MOCNESS tow between 40 and 80 m depth.

Parameter	Measured value	Acoustically inferred value
$\epsilon$ ( $\text{W kg}^{-1}$ )	$1 \times 10^{-7}$ – $1 \times 10^{-6}$	$5 \times 10^{-7}$
Animal length (cm)	1.47	1.5
Numerical density (animals $\text{m}^{-3}$ )	1	11

internal wave, however, Seim and Gregg (1994) measured values of  $\epsilon$  that occasionally exceeded  $1 \times 10^{-5} \text{ W kg}^{-1}$  in a set of shear billows that were 20-m tall. While the dynamics that generated this turbulence are different from those for an internal wave, the size and structure of the shear billows as measured by a scientific echosounder are similar to observations made of internal waves. Two other studies have estimated even larger dissipation rates for internal waves in the Scotian Shelf (Sandstrom *et al.*, 1989) and at the Equator (Hebert *et al.*, 1992) ( $\epsilon = 8 \times 10^{-6}$  and  $2 \times 10^{-5} \text{ W kg}^{-1}$ ).

A similar analysis was undertaken to estimate the length of biological scatterers. Theoretical scattering spectra were calculated for elongated, fluid-like scatterers with lengths ranging from 1 mm to 5 cm in increments of 0.5 mm

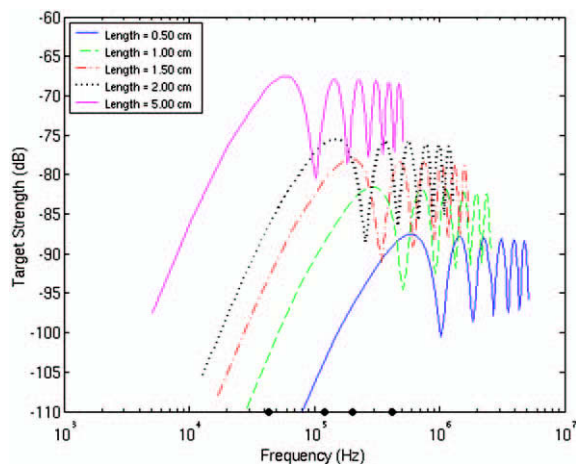


Figure 9. Theoretical scattering spectra for euphausiids ranging in length from 0.5 to 5.0 cm using Equation (1). Solid dots on the horizontal axis mark the acoustic frequencies used by BIO-MAPER-II.

(Figure 9). While many types of animals were caught in the MOCNESS tows, a “forward problem analysis” investigating the relative acoustic scattering by the various animals (similar to that done by Wiebe *et al.*, 1996) determined that euphausiids were the dominant scatterer in the water column. This approach uses the zooplankton information from net tows (animal type, numerical density for particular depth strata, and length) and physics-based scattering models to determine the overall level of biological scattering in the water column and the relative contributions from the different zooplankton taxa. From these results, only the euphausiids were subsequently modeled in the analysis.

The theoretical spectra with the best-fit to the measured spectra of the bottom layer of the internal wave was that of a 1.5-cm length, fluid-like animal (Figure 10). Results from the MOCNESS tow and subsequent “forward problem analysis” show that the dominant scatterers in the water column from 40 to 80 m deep were euphausiids (*Meganyctiphanes norvegica*). Copepods, amphipods, salps, and siphonophores were also present. The average length of the euphausiids caught in this depth range was 1.47 cm, with a standard deviation of 0.49 cm ( $n = 30$ ) (Table 3). The sub-surface layer (20–40 m depth) biomass was dominated by a huge abundance of salps. Salps are gelatinous animals and usually are assumed to be weak scatterers of sound, however, the validity of this assumption warrants further investigation.

Using the theoretical model for the scattering strength of a 1.5-cm long euphausiid, estimates can be made for the numerical density of these animals in this region. The difference in measured-scattering strength and that from the

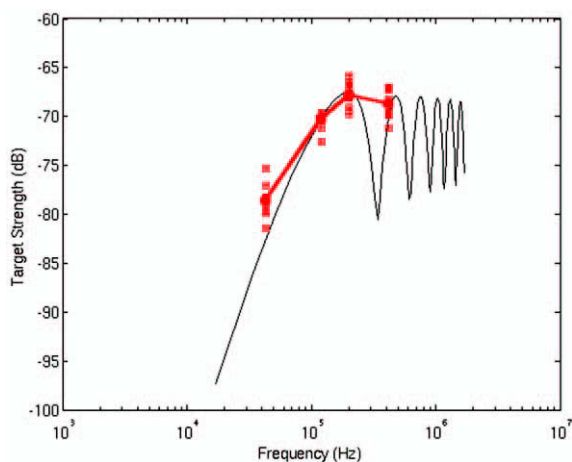


Figure 10. Measured scattering spectra from the lower layer of the internal wave (thick line) least-squares fit to the theoretical scattering spectra of a fluid-like zooplankton. Theoretical curves were offset in amplitude such that the fit was based only on the “turning point” of the curve which is a function of animal size. The theoretical curve with the best-fit was for a 1.5 cm long animal.

theoretical spectra for a single animal was 10.5 dB. An inversion using Equation (10) produces an estimate of 11 animals  $m^{-3}$  for the lower layer of the internal wave. Euphausiid numerical density estimated from net-tow data is approximately 1 animal  $m^{-3}$ . The discrepancy in these two estimates of numerical density may be explained by the assumptions used in the analysis. For the estimate from the inverse method, all the scattering in the water column is assumed to be from biological scatterers, all of which are assumed to be euphausiids. Thus, the acoustic estimate is an upper-limit of the numerical density of the animals. Conversely, the estimate from the net-tow data is a lower-limit since some animals present are likely to avoid capture by the MOCNESS (Wiebe *et al.*, 1982). Together these two estimates predict a range for the actual numerical density of animals in the water column.

The inverse methods that were used to calculate parameters of the scattering processes for the upper and lower layers of the internal wave were then applied through an automatic algorithm to the transect of the internal wave. Scattering was assumed to be from only one type of scattering process which was determined by the value of the slope parameter at each data point (Figure 5). The results of

this approach are maps of the following acoustically inferred parameters: dissipation rate of turbulent kinetic energy (Figure 11), euphausiid length, and numerical density of euphausiids (Figure 12). The estimates of these scattering parameters provide realistic values for both biological- and physical-scattering processes occurring in the internal wave. However, they are valid only in regions where one of the scattering processes is dominant, specifically in the part of the survey where the two layers of the internal wave are distinct.

## Discussion

Multiple-frequency acoustic systems can be used to survey regions of the ocean and may provide parameterizations of the biological and physical processes similar to those obtained with conventional sampling systems. Scattering spectra were distinguished to first-order by the slope of the scattering strength versus acoustic frequency in the Gulf of Maine in a region which had both biological scatterers and water-column microstructure. Certain regions were identified as being dominated by either a biological- or

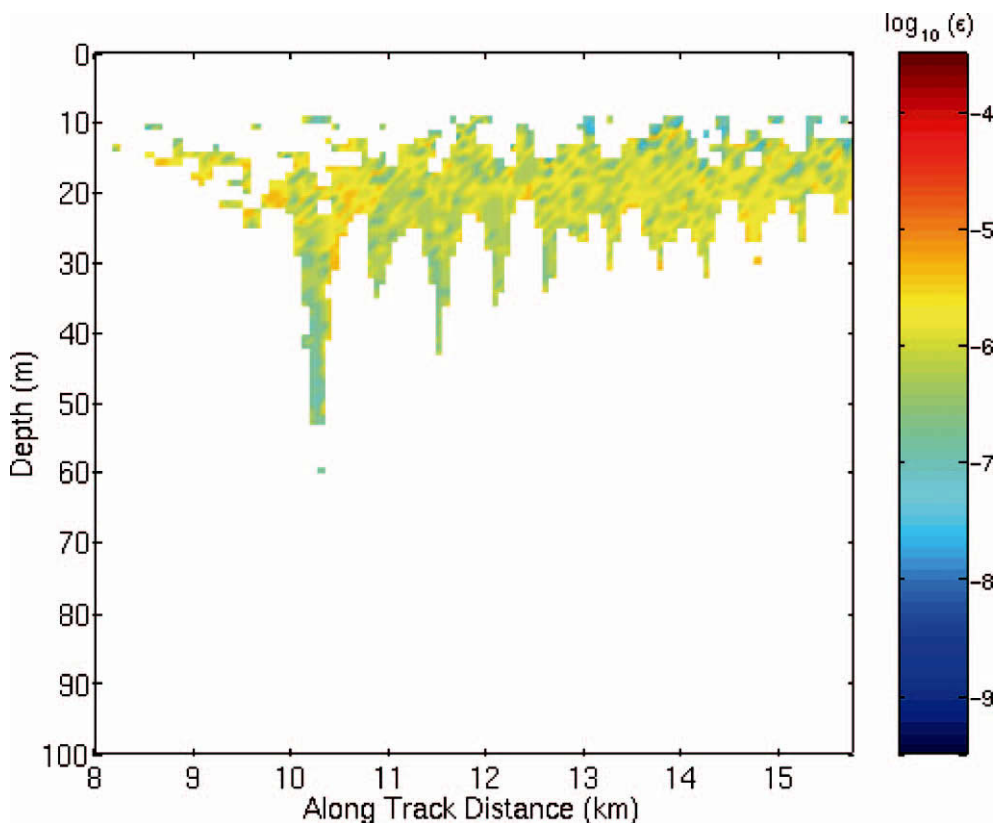


Figure 11. Dissipation rate of turbulent kinetic energy ( $\epsilon$ ) estimated by inverting multiple-frequency, acoustic-backscatter measurements. Data are only from points where the acoustic-spectral slope was less than  $-1.5 \times 10^{-5}$  dB  $Hz^{-1}$  (consistent with theoretical scattering from microstructure). Each data bin covers 1 m vertically and approximately 75 m horizontally.

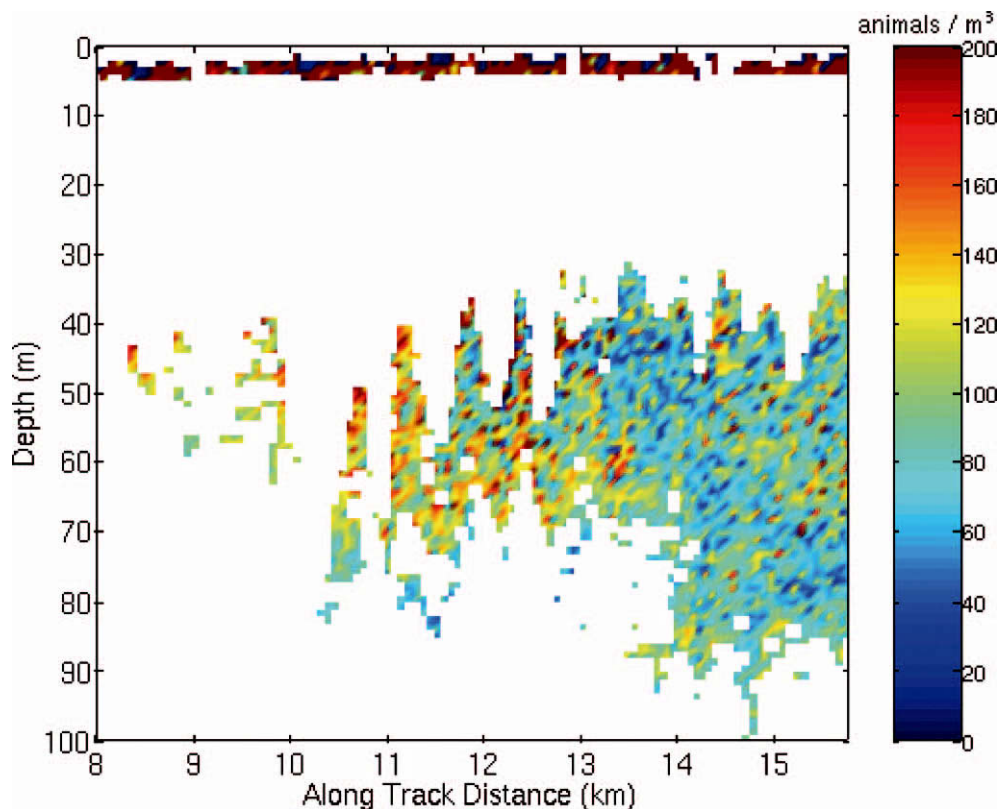


Figure 12. Numerical density of euphausiids found by inverting multiple-frequency, acoustic-backscatter measurements for animal length. The animal-length estimates are then used to determine the appropriate theoretical scattering curve, which is then inverted for estimates of numerical density of the animals. Data are only from points where the acoustic-spectral slope was greater than  $1.4 \times 10^{-5} \text{ dB Hz}^{-1}$  (consistent with theoretical scattering from biological organisms). Each acoustic data bin covers 1 m vertically and approximately 75 m horizontally. The data from 0 to 10 m depth may be contaminated by bubbles or surface waves.

physical-scattering process, however, large areas of the water column had spectra whose source could not be determined. Given the complexity of the oceanic environment, applicability of this differentiation technique will vary from region to region.

To obtain quantitative parameterizations, accurate physics-based models of the scattering can be used. For biological scattering, the animal which dominates the acoustic backscatter must be known via net sampling or direct observation. This is especially important when there are animals of many taxa present. In this study where euphausiids were the dominant biological scatterer, the turning point of the scattering spectra was used to estimate the length scale of the animal which agreed with measurements of net-collected animals. Differences in the relative amplitude of the measured and theoretical scattering spectra were used to estimate the numerical density of these scatterers. Given the assumptions of this approach, these estimates of numerical density should be taken as an upper bound of scatterer abundance.

The inversion of acoustic data for meaningful information of physical processes also requires accurate microstructure-

scattering models. The scattering model used in this work requires several inputs which describe the physical properties of the water column. High resolution CTD measurements and microstructure probes are the ideal way to provide these inputs. However, as this work has shown, the use of several assumptions may allow reasonable estimates of the dissipation rate of turbulent kinetic energy to be made from multiple-frequency, acoustic data. More rigorous testing of this approach needs to be undertaken where  $\varepsilon$  and  $\chi$  are measured instead of estimated. These measurements should be coincident with multiple-frequency, acoustic-backscatter data, hydrographic information, and net collections of the biological scatterers. Additional testing of the microstructure-scattering model should also be undertaken for both laboratory and field situations.

This approach demonstrates promise for synoptic discrimination and characterization of zooplankton and physical microstructure. Given the complexity of the problem, care needs to be taken in adapting this approach to other oceanographic regions with different levels of physical mixing processes and mixed assemblages of biological organisms. Finally, while the multiple-frequency acoustic system is

a powerful tool, direct measures of both zooplankton and temperature and salinity microstructure remain necessary as a means of ground-truthing the estimates from acoustic data.

## Acknowledgements

The Captain and crew of “Endeavor” were helpful and innovative in the deployment and recovery of BIOMAPER-II on her maiden voyage. Andy Girard, Tom Austin, Terry Hammer, Bob McCabe, Scott Gallager, and Tom Torkelson provided invaluable support to keep the instrument running. Andone Lavery provided model results and helpful manuscript criticism. Funding for BIOMAPER-II was provided by Office of Naval Research grants N00014-95-11102, N00014-98-1-0362, N00014-95-1-0287; and the U.S. GLOBEC Georges Bank program through NOAA grant #31654-5717. J.D.W. was supported by an Office of Naval Research graduate fellowship in ocean acoustics (N00014-00-1-0052) and the WHOI Education Office. This is Woods Hole Oceanographic Institution contribution number 10940 and U.S. GLOBEC contribution number 393.

## References

- Batchelor, G. K. 1959. Small-scale variation of convected quantities like temperature in turbulent fluid. Part I. General discussion and the case of small conductivity. *Journal of Fluid Mechanics*, 5: 113–133.
- Brierley, A. S., Brandon, M. A., and Watkins, J. L. 1998. An assessment of the utility of an acoustic Doppler current profiler for biomass estimation. *Deep-Sea Research Part I*, 45: 1555–1573.
- Castile, B. D. 1975. Reverberation from plankton at 330 kHz in the Western Pacific. *Journal of the Acoustical Society of America*, 58: 972–976.
- Davis, C. S., and Wiebe, P. H. 1985. Macrozooplankton biomass in a warm-core Gulf Stream ring: time-series changes in size, structure, and taxonomic composition and vertical distribution. *Journal of Geophysical Research*, 90: 8871–8884.
- Dietz, R. S. 1948. Deep scattering layer in the Pacific and Antarctic oceans. *Journal of Marine Research*, 7: 430–442.
- Dillon, T. M. 1982. Vertical overturns: a comparison of Thorpe and Ozmidov length scales. *Journal of Geophysical Research*, 87: 9601–9613.
- Foote, K. G., and Stanton, T. K. 2000. Acoustical methods. *In* ICES Zooplankton Methodology Manual (chapter 6), pp. 223–258. Ed. by R. Harris, P. H. Wiebe, J. Lenz, H. R. Skjoldal, and M. Huntley. Academic Press, London.
- Goodman, L. 1990. Acoustic scattering from ocean microstructure. *Journal of Geophysical Research*, 95: 11557–11573.
- Gregg, M. 1987. Diapycnal mixing in the thermocline: a review. *Journal of Geophysical Research*, 92: 5249–5286.
- Haury, L. R., Briscoe, M. B., and Orr, M. H. 1979. Tidally-generated internal-wave packets in Massachusetts Bay. *Nature*, 278: 312–317.
- Haury, L., Wiebe, P., Orr, W., and Briscoe, M. 1983. Tidally-generated, high-frequency internal-wave packets and their effects on plankton in Massachusetts Bay. *Journal of Marine Research*, 41: 65–112.
- Hebert, D., Moum, J. N., Paulson, C. A., and Caldwell, D. R. 1992. Turbulence and internal waves at the Equator. Part II: details of a single event. *Journal of Physical Oceanography*, 22: 1346–1356.
- Holliday, D. V., and Pieper, R. E. 1995. Bioacoustical oceanography at high frequencies. *ICES Journal of Marine Science*, 52: 279–296.
- Lennert-Cody, C. E., and Franks, P. J. S. 1999. Plankton patchiness in high-frequency internal waves. *Marine Ecology Progress Series*, 186: 59–66.
- McGehee, D. E., O’Driscoll, R. L., and Martin-Traykovski, L. V. 1998. Effects of orientation on acoustic scattering from Antarctic krill at 120 kHz. *Deep-Sea Research Part II*, 45: 1273–1294.
- Oakey, N. S. 1982. Determination of the rate of dissipation of turbulent energy from simultaneous temperature and shear microstructure measurements. *Journal of Physical Oceanography*, 12: 256–271.
- Oakey, N. S. 1988. Epsonde: an instrument to measure turbulence in the deep ocean. *IEEE Journal of Oceanic Engineering*, 13: 124–128.
- Orr, M. H., Haury, L. R., Wiebe, P. H., and Briscoe, M. G. 2000. Backscatter of high-frequency (200 kHz) acoustic wavefields from ocean turbulence. *Journal of the Acoustical Society of America*, 108: 1595–1601.
- Sandstrom, H., Elliott, J. A., and Cochrane, N. A. 1989. Observing groups of solitary internal waves and turbulence with BATFISH and echo-sounder. *Journal of Physical Oceanography*, 19: 987–997.
- Schmitt, R. W. 1994. Double diffusion in oceanography. *Annual Review of Fluid Mechanics*, 26: 255–285.
- Seim, H. E. 1999. Acoustic backscatter from salinity microstructure. *Journal of Atmospheric and Oceanic Technology*, 16: 1491–1498.
- Seim, H. E., and Gregg, M. C. 1994. Detailed observations of a naturally-occurring shear instability. *Journal of Geophysical Research*, 99: 10049–10073.
- Seim, H. E., Gregg, M. C., and Miyamoto, R. T. 1995. Acoustic backscatter from turbulent microstructure. *Journal of Atmospheric and Oceanic Technology*, 12: 367–380.
- Stanton, T. K., Chu, D., Wiebe, P. H., and Clay, C. S. 1993. Average echoes from randomly-oriented, random-length finite cylinders: zooplankton models. *Journal of the Acoustical Society of America*, 94: 3463–3472.
- Stanton, T. K., Wiebe, P. H., Chu, D., Benfield, M. C., Scanlon, L., Martin, L., and Eastwood, R. L. 1994a. On acoustic estimates of zooplankton biomass. *ICES Journal of Marine Science*, 51: 505–512.
- Stanton, T. K., Wiebe, P. H., Chu, D., and Goodman, L. 1994b. Acoustic characterization and discrimination of marine zooplankton and turbulence. *ICES Journal of Marine Science*, 51: 469–479.
- Stanton, T. K., Chu, D., and Wiebe, P. H. 1998. Sound scattering by several zooplankton groups. II. Scattering models. *Journal of the Acoustical Society of America*, 103: 236–253.
- Thorpe, S. A. 1987. Transitional phenomena and the development of turbulence in stratified fluids: a review. *Journal of Geophysical Research*, 92: 5231–5248.
- Trevorrow, M. V. 1998. Observations of internal solitary waves near the Oregon coast with an inverted echo sounder. *Journal of Geophysical Research*, 103: 7671–7680.
- Wiebe, P. H., Boyd, S. H., Davis, B. M., and Cox, J. L. 1982. Avoidance of towed nets by the euphausiid *Nematoscelis megalops*. *Fishery Bulletin*, 80: 75–91.
- Wiebe, P. H., Morton, A. W., Bradley, A. M., Backus, R. H., Craddock, J. E., Barber, V., Cowles, T. J., and Flierl, G. R. 1985. New developments in the MOCNESS, an apparatus for sampling zooplankton and micronekton. *Marine Biology*, 87: 313–323.
- Wiebe, P. H., Mountain, D. G., Stanton, T. K., Greene, C. H., Lough, G., Kaartvedt, S., Dawson, J., and Copley, N. 1996.

- Acoustical study of the spatial distribution of plankton on Georges Bank and the relationship between volume-backscattering strength and the taxonomic composition of the plankton. *Deep-Sea Research Part II*, 43: 1971–2001.
- Wiebe, P. H., Stanton, T. K., Benfield, M. C., Mountain, D. G., and Greene, C. H. 1997. High-frequency acoustic-volume backscattering in the Georges Bank coastal region and its interpretation using scattering models. *IEEE Journal of Oceanic Engineering*, 22: 445–464.
- Wiebe, P. H., Stanton, T. K., Greene, C. H., Benfield, M. C., Sosik, H. M., Austin, T., Warren, J. D., and Hammer, T. 2002. BIOMAPER II: an integrated instrument platform for coupled biological and physical measurements in coastal and oceanic regimes. *IEEE Journal of Oceanic Engineering*, 27: 700–716.
- Woods, J. D. 1977. Turbulence as a factor in sound scattering in the upper ocean. *In* *Oceanic Sound Scattering Prediction*, pp. 129–145. Ed. by N. R. Andersen, and B. J. Zahuranec. Plenum Press, New York.